SEASONAL-TO-INTERANNUAL FLUCTUATIONS IN SURFACE TEMPERATURE OVER THE PACIFIC: EFFECTS OF MONTHLY WINDS AND HEAT FLUXES

Daniel R. Cayan[1], *Arthur J. Miller*[1], *Tim P. Barnett*[1], *Nicholas E. Graham*[1], *Jack N. Ritchie*[1], *and Josef M. Oberhuber*[2]

ABSTRACT

Monthly heat fluxes and wind stresses are used to force the Oberhuber isopycnic ocean general-circulation (OPYC) model of the Pacific basin over a two-decade period from 1970 to 1988. The surface forcings are constructed from COADS marine observations via bulk formulae. Monthly anomalies of the fluxes and stresses are superimposed upon model climatological means of these variables, which were saved from a long spin-up. Two aspects of this work are highlighted, both aimed at a better understanding of the atmosphere-ocean variability and exchanges and at diagnosing the performance of the OPYC model in simulating monthly to decadal-scale variability. The first is the evaluation of the data used to force the model ocean, along with its relationship to other observed data. The second is the diagnosis of the processes revealed in the model that are associated with sea surface temperature (SST) variability, including their seasonal and geographic structure.

Although both random and systematic errors arise from the marine data and the bulk formulations, large signals in the air-sea fluxes are nonetheless consistent with the large-scale atmospheric circulation anomalies over the Pacific. This signal is large in a composite prepared from months with similar circulation modes. Also, latent and sensible heat-flux anomaly patterns correspond well to those of SST anomaly tendencies. Considering short-period variations, SST anomaly tendencies have typical magnitudes of 0.3°C mo^{-1}. These are associated with monthly mean flux anomalies having typical magnitudes of 50 W m^{-2} and are consistent with observed mixed-layer depths. Decadal anomalies have much smaller magnitudes, perhaps reduced by two orders of magnitude, and it is here that the signal-to-noise problem is more severe. The forcing terms are generally products of variables, so realistic means and fluctuations of these variables are crucial for a successful simulation.

The 19-year simulation of the Pacific basin by the monthly marine data-forced OPYC model displays good skill in reproducing SST variability. These results represent the first

[1] Scripps Institution of Oceanography, University of California, San Diego, La Jolla, California
[2] Max-Planck-Institut für Meteorologie, Hamburg, Germany

hindcast of which we are aware that uses both observed total heat-flux and wind-stress anomalies as forcing for such a long time interval. There is close agreement between the model SSTs and those observed in many regions of the Pacific, including the tropics and the northern extratropics. Besides performing credibly on the monthly time scale, the model captures the essence of low-frequency variability over the North Pacific, including aspects of a marked basin-wide change that occurred in 1976-1977. In the model's detailed heat budget, the anomalous air-sea heat fluxes, entrainment, and to a lesser extent horizontal advection, force thermal-anomaly changes in the mixed layer. Each of these components was apparently involved in the 1976-1977 decadal SST shift.

INTRODUCTION

Our purpose is to describe monthly to decadal variations in surface variability over the Pacific basin. The results presented combine a historical set of monthly marine observations and a two-decade numerical simulation (Miller et al., 1994a,b) that uses the Oberhuber (1993) isopycnic ocean general-circulation model.

The first part of the paper is an analysis of observed monthly surface marine atmospheric variability in relation to sea surface temperature (SST) over the Pacific Ocean. This observational evidence provides background to the second section of the paper, in which monthly wind stresses and heat fluxes are used to force an ocean general-circulation model (OGCM). In the observational section, we concentrate on the variability of the latent and sensible heat fluxes, since they provide a good example of the characteristics and problems involved in bulk formulations using the marine data. The fluxes exhibit monthly variability with large-scale organization, and their effect on the ocean can be detected in the monthly fluctuations of the SST anomaly field.

The second part of the paper reports on applying the marine data parameterizations to a simulation over two decades (1970-1988) of the Pacific Ocean basin using the OPYC OGCM. This run is forced by monthly mean wind stress and fluxes derived from surface marine observations, which are introduced in the first section. In assessing this run, we compare the model SST anomalies with observations, particularly their low-frequency variability. Further insight is provided by the model upper-ocean heat budget, which is not well described by observations.

Aside from diagnosing mechanisms causing monthly SST variability, one motivation for this simulation was to better understand a strong regime-like change in SST that occurred in the North Pacific basin during the mid-1970s (Douglas et al., 1982; Nitta and Yamada, 1989; Trenberth, 1990; Miller et al., 1994a,b; Graham, 1994; Trenberth and Hurrell, 1995, in this volume). Although thorough observational documentation of decadal-scale variability is lacking, glimpses from recent historical episodes suggest that this "gray area" (Karl, 1988) of the variability spectrum contains important climate effects. The actual shift was identified in fall and winter of 1976-1977 when SSTs in the central North Pacific cooled markedly and SSTs along the west coast of North America warmed (Venrick et al., 1987; Trenberth, 1990; Ebbesmeyer et al., 1991). In the atmosphere, the shift involved a basin-scale deepening of the wintertime Aleutian Low System, and appears to have been at least partially instigated by forcing from the tropical Pacific (Graham, 1994; Trenberth, 1995, in this volume), although an alternative theory involves sea-air feedback and advection of thermal anomalies by the North Pacific subtropical gyre (Latif and Barnett, 1994). Accompanying changes in many other physical and biological variables in the North Pacific basin and around its margin were also noted (Venrick et al., 1987; Ebbesmeyer et al., 1991).

The bulk formulae parameterized heat fluxes, calculated from standard marine surface meteorological observations, are the only means of estimating a multi-year time history of the heat exchange over broad regions of the oceans. Similarly, SST has been measured routinely by merchant ships for several decades, and, in the absence of a comprehensive temperature-versus-depth set in the upper ocean, SST is used to infer the variability of the upper-ocean heat content. Although the ocean heat-content structure can be complex, during winter in the extratropics the upper ocean is quite well mixed and SST is a good indicator (White and Walker, 1974).

As is brought out in the section below, there is a rich variability, superimposed upon the climatological mean, that involves both atmospheric and oceanic fluctuations. Three tests of the surface heat budget are discussed here. The first two, which study the data directly, are to relate monthly anomalies of the latent and sensible fluxes to the anomalous atmospheric circulation and to anomalous tendencies of the SST field. The third is to incorporate the monthly bulk-formula wind stress and heat flux as forcing of an extended OGCM run and to compare the simulated versus the observed SST fields. These results represent the first hindcast of which we are aware that uses both observed total-heat-flux and wind-stress anomalies as forcing for such a long time interval.

OBSERVATIONAL EVIDENCE FOR ANOMALOUS AIR-SEA HEAT EXCHANGE

Data

The primary data employed in the observational section of this study, as well as in the model forcing, are gridded

monthly mean ship-observed marine surface data for 1946-1986 from the Comprehensive Ocean-Atmosphere Data Set (COADS) (Slutz et al., 1985; Woodruff et al., 1987). From this set, several variables are employed, including the scalar wind or wind speed w, west-to-east and south-to-north horizontal surface wind components $u,v,$ sea level pressure (SLP), specific humidity q_a, air temperature $T,$ and sea surface temperature SST. Derived variables include the products $\{w\Delta T\}$, $\{w\Delta q\}$, $\{wu\}$, and $\{wv\}$, where the monthly averages of products of the individual observations are indicated by { }. These products are involved in parameterizing the sensible and latent heat flux, and the horizontal wind-stress components, respectively.

To reduce errors in the data fields and condense the number of data in the analyses, the COADS 2°-gridded "Monthly Summaries Trimmed" data were averaged onto 5° squares, centered at 5° latitude-longitude intersections. This averaging was applied to the anomalies of the 2° squares, rather than their values, to avoid spurious 5° anomalies caused by poor sampling within the domain. Long-term means employed were calculated over 1950 to 1979. Details are provided in four papers by Cayan (1990; 1991, hereafter designated DC1; 1992a, designated DC2; and 1992b, designated DC3).

Bulk Formula Parameterizations

Latent and sensible heat exchange at the ocean surface is an important mechanism for venting ocean heat absorbed from solar radiation to the atmosphere. Globally, approximately 60 percent of the solar radiation absorbed at the earth's surface is released by latent and sensible heating, primarily from the ocean (Sellers, 1965). Gill and Niiler (1973) invoked scaling arguments in the governing equations to infer that, over large scales (≥ 1000 km meridionally and ≥ 3000 km zonally), anomalous open-ocean surface temperature changes are dominated by changes in heat fluxes through the surface, rather than by advective influences. Since they depend on both oceanic and atmospheric conditions, the latent and sensible fluxes vary strongly over space and time. In the extratropics, latent and sensible fluxes are greatest in fall and winter when the near-surface vertical gradients of humidity and temperature are largest and wind speeds are highest (Esbensen and Kushnir, 1981; Isemer and Hasse, 1985, 1987).

The bulk aerodynamic formulae used for the latent and sensible heat fluxes are

$$Q_l = \rho L C_E \{w\Delta q\} \quad (1)$$

and

$$Q_S = \rho c_p C_H \{w\Delta T\}, \quad (2)$$

where Q_l is the latent flux, Q_S is the sensible flux, L is the latent heat of evaporation of water, and c_p is the specific heat of air at constant pressure. Again, w is the wind speed, Δq is sea surface saturation minus air specific humidity, and ΔT is SST minus air temperature. C_E and C_H are the transfer coefficients for latent heat and sensible heat, respectively, and are taken to be the modified Bunker coefficients given by Isemer and Hasse (1987). Unlike their mean values (Blanc, 1985), the anomalies of the fluxes are not particularly sensitive to the choice of exchange coefficients. A comparison of monthly anomalies obtained with these exchange coefficients to those from two other schemes yielded strong agreement (DC2).

The sense of the latent and sensible fluxes adopted throughout the paper is *positive* for heat *entering* the ocean from the atmosphere.

Errors in the Latent and Sensible Fluxes

Because of uncertainties in the bulk formulae and because the marine data have inaccuracies and are non-uniformly measured, the parameterized flux estimates contain errors. Although it is not possible to determine precisely the spatial and temporal characteristics of errors in the bulk-formulae-derived heat fluxes, estimates of their magnitudes have been attempted. In many regions the aggregate of the errors in the fluxes considerably exceeds the 10 W m^{-2} tolerance that has been targeted for climate studies (Taylor, 1984). Nevertheless, it will be shown that important climate variability (monthly to decadal time scales) is still contained in the flux estimates. A review of individual monthly maps of the fluxes finds that several have anomalies with magnitudes of 50 W m^{-2} or greater, a "signal" which is well beyond reasonable error estimates. From our observational and modeling experience, the character of this error, as much as its magnitude, is crucial. For example, a 10 W m^{-2} error is probably acceptable if it has a high-frequency, random variability, but it is intolerable if it has low-frequency (decadal-scale) changes.

Both random and systematic errors in marine observations and errors in the bulk formulae contaminate the monthly mean fluxes (Weare, 1989; Taylor, 1984; DC1). Random measurement errors and errors from incomplete sampling of the natural weather fluctuations are reduced by averaging several observations together. Because the mean of the fluxes was removed and the resulting anomalies are generally only a fraction of the mean, the non-time-varying biases are reduced considerably. The largest random errors in the flux estimates appear to be caused by sampling variability, and to a lesser extent by observation errors (DC1). This error was estimated by a Monte Carlo sampling exercise (DC1) where the mix of observations entering particular flux estimates within well-sampled regions was repeatedly re-sampled. The uncertainty of the monthly mean for well-sampled 5° squares (50 or more independent samples per month) is reduced to approximately 40 W m^{-2} or less for

the latent flux and to 20 W m^{-2} or less for the sensible flux. The density of observations is relatively high over the extratropics of the North Pacific and North Atlantic, with many 5°squares having 100 or more observations per month. However, the density is marginal-to-poor over the tropics and in the Southern Hemisphere, with fewer than 20 observations per month at many 5° squares. In these sparsely sampled regions, random errors in the monthly flux estimates are likely to be substantial. Consequently, in forcing the OGCM in the region between 20°N and 20°S and data-poor regions south of 20°S, we have resorted to a Newtonian damping scheme for the net flux anomalies.

Systematic errors are caused by biases in the bulk formulae and in the observations, and are not automatically reduced by averaging. Time-varying biases in the fundamental observations caused by changes in instrumental practices are probably a significant source of error. These errors are difficult to quantify, but the marine data have "global" (over the available COADS-covered region) trends in w and ΔT, which translate to changes of approximately 0.8 m s^{-1} and −0.2°C over 1950 to 1986. Because these seem to be at least partially caused by instrument and calibration changes over the period, the fluxes were adjusted to remove the effects of the global average linear trends. This adjustment reduced the linear change in the latent and sensible fluxes over 1950 to 1986 by about 20 W m^{-2} and 5 W m^{-2}, respectively (DC1 and DC2). This adjustment has only minor influence on the high-frequency variability, but it does significantly affect the multi-year numerical model run, because the effects are cumulative. More discussion of the systematic errors in the marine data is provided below.

Anomalous Variability of the Heat-Flux Components

The dependence of the flux anomalies on the mean conditions and the anomalies of the fundamental surface variables was explored in DC1. For the monthly latent flux anomaly where an overmark indicates the long-term monthly mean and a prime indicates the monthly anomaly. For monthly means, most of the variation comes from w and Δq, not from the exchange coefficients (DC1). The last term on the right-hand side of (3) does not contribute strongly to latent flux anomalies, because w and Δq monthly anomalies are not locally well correlated over most of the oceans (DC1). A similar relationship involving ΔT instead of Δq describes the monthly sensible flux anomalies.

$$Q'_l \sim \overline{w}\Delta q' + w'\overline{\Delta q} + w'\Delta q' , \qquad (3)$$

Equation (3) shows that the joint behavior of mean values and anomalies of wind speed w, the ocean-surface saturation humidity-air humidity difference Δq, and the sea-air temperature difference ΔT must be included to determine the flux anomalies. For atmosphere-ocean models, this interplay between the mean and anomaly components is a challenge. It is not enough to simulate anomalies of w, Δq, and ΔT; their mean fields must also be properly represented.

There are strong seasonal and geographical modulations of the flux anomalies. In the extratropics the variance is greatest in fall and winter when w, Δq, and ΔT have largest mean values and strongest variability. The largest contributions to the extratropical variance of Q_l anomalies involve $\overline{w}\Delta q'$. Anomalies of Q_s become important north of about 35°N, where their variance is dominated by the term involving $\overline{w}\Delta T'$. In the extratropics, the variance of each of these components is maximum along the western side of the basin, because strong ocean boundary currents and large air-mass differences between the upwind land mass and the sea cause great contrasts. Latent flux anomalies in the tropics often involve greater contributions from $w'\overline{\Delta q}$ than do those in mid-latitudes, although the eastern tropical Pacific has relatively large contributions from $\overline{w}\Delta q'$.

The Δq and ΔT monthly anomalies are correlated (cooler air is usually drier), especially in the extratropics, so the latent and sensible anomalies usually reinforce each other, yielding relatively large net heating anomalies. In the extratropics, flux anomalies are linked to the local wind direction, but in the tropics they are usually not (DC2). North of about 15°N, the largest positive anomalies are associated with northerly to northwesterly winds; they probably result from meridional advection of atmospheric humidity and temperature, and also from changes in the strength of the westerly winds. In the tropics, there is little relationship between wind direction and the flux anomalies, since horizontal gradients of humidity and temperature are weak and the wind direction is relatively steady.

How does the variability of the anomalous latent and sensible fluxes compare with that of the radiative fluxes? The balance of the heat-flux anomaly terms is distinctly different from that of the mean terms. Combined anomalies of Q_l and Q_s often exceed 50 W m^{-2} over regions several hundred kilometers in extent (DC1 , DC2, and DC3). These estimates indicate that monthly anomalies of Q_l and Q_s are usually larger than those of the radiative components. Comparing the variances of Q_l and Q_s, with those of bulk-formulae-estimated net solar radiative flux Q_{sw} and infrared flux Q_{IR}, DC1 found that: (1) Q_l and Q_s, anomalies dominate the monthly anomalous surface heat budget during winter in the extratropics north of 30°N, (2) Q_l anomalies dominate from about 15°N to about 30°N, and (3) Q_l and Q_{sw} anomalies are about equally large from 15°N to 15°S.

Flux Anomalies and Atmospheric Circulation

Q_l and Q_s anomalies have regional-to-basin-scale coherence both the North Atlantic and North Pacific. The first four empirical orthogonal functions (EOFs) of the sum of the Q_l and Q_s anomalies (Q'_{l+s}) account for about half of the total variance of this field in each basin (DC1). That these

patterns relate to the anomalous atmospheric circulation is evidence for a realistic flux-anomaly signal. The dominant atmospheric-circulation anomaly modes in the North Atlantic and North Pacific, represented as EOFs of the sea level pressure, produce systematic flux-anomaly patterns (DC2). The first SLP EOF in the North Pacific features a large pressure anomaly in the central North Pacific, and is associated with the well-known "Pacific-North American" (PNA) pattern. Three correlation fields linking the PNA to surface variables are shown in Figure 1: the correlations between winter-month PNA time amplitudes and gridded fields of w (wind speed), Δq, and Q_{l+s} anomalies. This set of maps, and others in DC2, show that the anomaly fields of w, Δq, and latent-plus-sensible flux are remarkably consistent with major SLP anomaly patterns over the North Pacific and North Atlantic. Negative SLP anomalies favor positive w anomalies to their south and negative w anomalies to their north, associated with shifts in storm tracks and changes in the mean wind field. Negative SLP anomalies favor positive Δq (and ΔT) to their west, and negative Δq to their east, probably because of meridional advection of air temperature and humidity. The flux anomalies are a hybrid of these patterns, with enhanced sea-to-air fluxes to the southwest and diminished fluxes to the east of negative SLP anomalies.

For the strong Aleutian low phase of the PNA, the anomalous wind-speed field is dominated by a single zonally oriented high-wind patch to the south of the Low in the central North Pacific, with out-of-phase tendencies to the north and the south. Δq and ΔT anomalies are arranged in pockets to the southwest (positive anomalies) and to the east (negative anomalies) of the low. Farther afield, a positive anomaly center appears in the Gulf of Mexico, reflecting the well-known downstream teleconnection of deep troughs and cold dry air outbreaks leading to positive ΔT and Δq anomalies over the southeast United States. The pattern has a broad center of positive anomalies to the southwest of the Aleutian Low, and a region of negative anomalies east of the Low along the West Coast. In the section of this paper that reports on the ocean model, it is shown that low-frequency changes in the PNA between the 1960s and 1980s were associated with marked variations in heat flux and wind stress, which produced striking variability in the upper-ocean thermal structure.

Flux Anomalies and SST

Does the heat flux drive the SST, or does the SST drive the heat flux? The relationship between SST and the climatological mean of total latent and sensible heat flux appears to support two different points of view. On one hand, the fluxes may be *driven* by the SST: High ocean-to-atmosphere fluxes are found in the tropics where there is warm water and high saturation-vapor pressure, and low fluxes occur in high latitudes and along the eastern side of the ocean basins where surface temperatures are cool. Concerning the anomaly relationships, there is evidence for the SST-forcing-flux mechanism in the warm-season extratropics and in the tropics (Cayan, 1990; Liu and Gautier, 1990).

On the other hand, in the extratropics the fluxes appear

to force the temperature (Gill and Niiler, 1973; DC3): SST is coolest in late winter following the highest ocean-to-atmosphere fluxes. For the flux-forcing-SST case to be valid, the SST anomaly must play a negligible role in determining the flux, so that the flux is driven by atmospheric conditions—i.e., w, T_a, and q variations dominate the variations of SST. Indirectly, this scenario has been investigated by relating SST anomalies to the large-scale atmospheric circulation (Namias, 1972; Davis, 1976; Wallace et al., 1990). While all of these studies established a definite connection between the monthly or seasonal mean circulation and the SST anomalies, they could only infer the role of anomalous heat flux in forcing SST anomalies. When atmospheric fields are related to contemporaneous monthly SST anomalies, it is difficult to determine whether SST is forcing the atmosphere, both fields are being forced by some other agent, or the atmosphere is forcing the SST.

In testing the phase relationship between anomalies of the estimated flux and SST, the dominant linkage exhibited in the extratropics is that the latent and sensible flux anomalies force the SST anomalies, rather than SST anomalies' forcing the flux anomalies (DC3). Historical time series of flux data provide the basis for directly testing the forcing. Correlations between bulk formulae fluxes and anomalous temperature variations have been documented over the North Pacific by Clark et al. (1974) and Frankignoul and Reynolds (1983), and in the western tropical Pacific by Meyers et al. (1986). As was reported in DC3, the latent and sensible heat-flux anomalies proved to strongly affect monthly changes in SST anomalies over a large portion of the world oceans, in particular the North Atlantic and the North Pacific. A simple thermodynamic model was adopted to relate the flux anomalies to the *tendency* (time rate of change) of the SST anomalies. More discussion of the full mixed-layer thermodynamic equation is given below, and a comprehensive treatment is provided by Frankignoul (1985). Note that the temperature equation predicts the *tendency* of the SST anomaly $\frac{\partial SST'}{\partial t}$, not the anomaly itself; the tendency is represented here by its finite-difference forms, $\frac{\Delta SST'}{\Delta t}$. The flux parameterizations do not contain knowledge of the SST tendency, so the relationship of fluxes to SST-tendency anomalies is an independent test of the influence of the fluxes.

Having a higher-frequency character than the anomaly itself, $\frac{\Delta SST'}{\Delta t}$ has nearly as many independent samples of $\frac{\Delta SST'}{\Delta t}$ as there are months; four decades of records contain approximately 120 independent December-January-February samples.

Spatial Distribution of Flux versus SST Tendency Anomalies

The geographical distribution of the correlations between Q'_{l+s} and $\frac{\Delta SST'}{\Delta t}$ observations for winter months is examined in Figure 2. The 0.3 level is used as a threshold of statistical significance. Meaningful correlations on this map are almost everywhere positive, as they were for zonal averages of the two fields (DC3). Strongest correlations (^{3} 0.5) are found mostly between about 25°N and 40°N within the anticyclonic subtropical gyres of the two oceans. For the North Pacific, strongest correlations are east of 180° and extend to the California Current. Though significant in many locations, correlations are weaker in the western North Pacific and from the tropics to 30°S. In the central North Atlantic, the flux and $\frac{\Delta SST'}{\Delta t}$ anomalies have strong correlations in the central subtropical gyre as well as in the high-variance western North Atlantic region. Seasonally, most of the regions have strongest correlations in winter.

Near the equator between 5°N and 5°S in all three basins, Q'_{l+s} and $\frac{\Delta SST'}{\Delta t}$ are not well correlated. Correlations between zonal average flux and SST anomalies (DC3; not shown) indicate that in the tropics, the flux and SST anomalies (not the tendencies) tend to be negatively correlated. This suggests that the flux is driven by SST, presumably because equatorial SST anomalies are governed more by internal ocean processes than by the air-sea heat exchange.

$\frac{\Delta SST'}{\Delta t}$ versus Fluxes during Strong Atmospheric-Circulation Modes

The organization of the latent-plus-sensible flux anomalies (Q'_{l+s}) by the anomalous atmospheric circulation can be used to test the consistency of large-scale links between the flux and SST tendency anomalies $\frac{\Delta SST'}{\Delta t}$ If the SST tendency anomalies are caused by the fluxes, they should have corresponding patterns. In DC3, the organization by the circulation was exploited by using the dominant SLP EOF modes as an index to compare flux-anomaly and corresponding SST-anomaly tendency patterns.

To identify strong winter-circulation months, extreme positive and negative EOF amplitudes were chosen for each SLP EOF (DC2 and DC3). Using this criteria, several (10-30) months of each of the extreme EOF modes (positive and negative amplitudes) were selected. Composites of Q'_{l+s} and $\frac{\Delta SST'}{\Delta t}$ were formed by averaging the fields during the respective extreme months. For brevity, the composites were expressed as the difference between averages of positive (strong) and negative (weak) phase months of the SLP EOFs.

In both northern oceans, the patterns of $\frac{\Delta SST'}{\Delta t}$ are well aligned with the flux anomaly patterns. In the North Pacific, composite $\frac{\Delta SST'}{\Delta t}$ differences and Q'_{l+s} differences corresponding to positive-minus-negative extremes of the PNA pattern are shown in Figure 3. Remarkably, the flux and $\frac{\Delta SST'}{\Delta t}$ signatures of the PNA are marked out more than halfway around the hemisphere. Major centers of $\frac{\Delta SST'}{\Delta t}$ are closely matched to those of Q'_{l+s} which confirms that

they are causally linked. At the centers, differences exhibit magnitudes of 0.2°C mo^{-1} to 0.8°C mo^{-1}. Corresponding flux differences range from about 30 to 120 W m^{-2} Over the North Pacific, the PNA incorporates a swath of positive Q'_{l+s} differences across mid-latitudes (centered at 40°N) from Asia to 140°W, and an arc of negative Q'_{l+s} differences extending from the subtropics at 20°N, 160°E to the eastern North Pacific border, from California to the Gulf of Alaska. Downstream, the strong downstream arm of the PNA produces negative Q'_{l+s} differences in the Gulf of Mexico and the eastern seaboard of the United States, and positive anomalies in the subtropical North Atlantic (20°N, 50°W) and east of Newfoundland. Throughout the North Pacific and North Atlantic, the PNA-associated $\frac{\Delta SST}{\Delta t}$ differences mirror the flux differences, having centers co-located with the flux differences. Magnitudes of the corresponding flux and SST anomaly tendencies are consistent with typical observed mixed-layer depths, approximately 100 to 250 m in winter and 10 to 40 m in summer. Similar seasonal behavior and the relation between the flux and SST tendency are replicated in the OGCM, as presented in the following section.

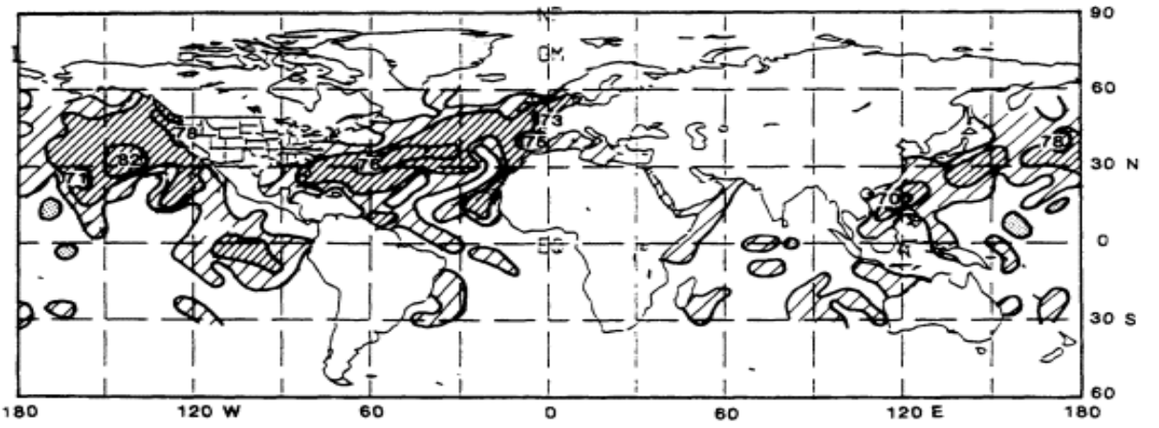

Figure 2
Correlation coefficients (×100), mapped for global ocean Q'_{l+s} vs. $\frac{\Delta SST}{\Delta t}$ at each grid point, for the winter months, 1946-1986. Contours at 0.3, 0.5, and 0.7. Light and heavy shadings indicate correlations ≥0.3 and ≥0.5.

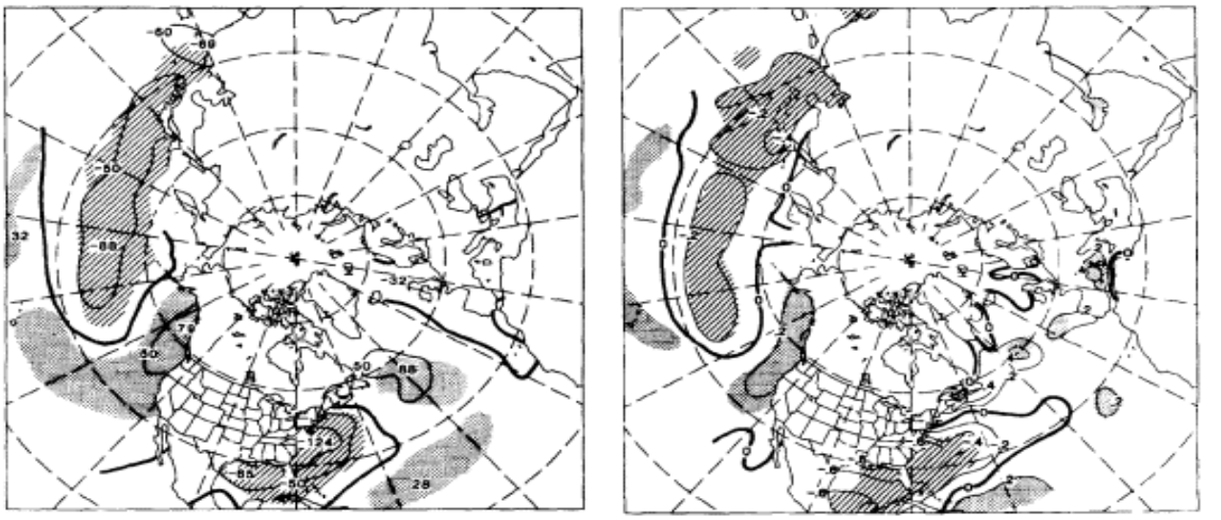

Figure 3
Difference of composites of Q'_{l+s} (W m^{-2}; left) and $\frac{\Delta SST}{\Delta t}$ (°C mo^{-1}; right) associated with positive (deep Aleutian Low phase) vs. negative extremes of EOF I of North Pacific SLP. Shading indicates regions where the difference exceeds the 95 percent confidence limit using a two-tailed t-test.

OCEAN MODEL

In this section, we report on an extended run of the OPYC OGCM, which was forced by the wind stress and fluxes derived from the surface marine observations (see Miller et al., 1994a,b). The OPYC model, developed by Oberhuber (1993), consists of eight isopycnal interior ocean layers fully coupled to a surface bulk mixed-layer model, the latter also including a sea-ice model. The interior layers (fixed potential density) and the mixed layer (variable density) have prognostic thicknesses that vary as a function of space and time; the interior layers may have zero thickness, and the mixed layer has a minimum thickness of 5 m. The interior potential densities are specified in such a way as to yield increased vertical resolution (thinner layers) in the thermocline and less in the deep ocean (thick layers). The low horizontal resolution perforce disallows mesoscale eddy variability, which is probably unimportant in the evolution of large-scale SST anomalies. The ocean model solves the full primitive equations for mass, velocity, temperature, and salt for each layer in spherical geometry with a realistic equation of state. The domain is the Pacific Ocean from 70°S to 65°N and 120°E to 60°W. The grid resolution is 77 by 67 points. Resolution is enhanced near the equator and near the eastern and western boundaries. Open-ocean resolution in the middle latitudes is 4°, which is suitable for examining the large-scale variability. The conditions on horizontal solid boundaries are no-slip for velocity and thermally insulating for temperature. The model's Antarctic Circumpolar Current, however, has periodic boundary conditions and unrealistically connects to itself from 60°W to 120°E (half the global circumference). The surface boundary conditions for interior flow are determined by the bulk mixed-layer model, which is forced by the atmosphere. Frictional drag acts between each layer but most strongly along the bottom boundary, which has realistic topography. Horizontal Laplacian friction and diffusion with variable coefficients are also included.

A full discussion of the dynamics is given by Oberhuber (1993), who used the model in Atlantic Ocean modeling studies, and by Miller et al. (1992, designated MOGB below), who used an earlier version of this model for tropical Pacific Ocean circulation studies. Besides the differences in geometry and the forcing functions to be described, the present model differs from MOGB in the following ways: A horizontal finite-differencing scheme based on Bleck and Boudra (1981) that conserves both enstrophy and potential vorticity is implemented in this version of the model. In addition, for a more realistic mixed-layer depth (MLD) in the middle latitudes, the mean turbulent kinetic energy (TKE) input into the mixed-layer equation for entrainment velocity has been altered to provide for month-to-month variability, and is lower than that of the MOGB model. The net result is to reduce the MLD in the middle and high latitudes of the North Pacific relative to that of MOGB, with the present values being more typical of those observed.

Concerning the OPYC ocean general-circulation model, it is important to point out some potential defects that may obscure our interpretations (Miller et al., 1994a). First, horizontal advection may be underestimated because the model SST climatology is too weak, especially in the Northwest Pacific. Second, the Kuroshio is not well resolved, so the model cannot generate strong western boundary currents. This will impair its ability to advect SST anomalies to nearby open ocean regions. Third, a warm bias in the model winter SST field (approximately 4°C too warm) in the northern North Pacific results in an overly stable stratification that diminishes the effects of entrainment. Last, salinity variations were not included, and these may be important, particularly in high latitudes. Although the OPYC OGCM's rather low resolution has excluded the effects of oceanic mesoscale variability on SST anomaly generation, we expect that such anomalies would have spatial scales too small to provoke important reactions in the large-scale atmospheric fields (Klein and Hua, 1988; Halliwell and Cornillon, 1989; Miller, 1992).

Forcing Functions and Model Runs

Since no ocean model is perfectly realistic, any model forced by observed total heat fluxes (without any feedback) will establish an oceanic temperature climatology that will depart from the real observations. To circumvent this problem, we forced the model with observed *anomalies* of heat fluxes superimposed upon the model climatology rather than with the total observed flux fields. This scheme preserves the model ocean climatology, as follows. We first establish the model climatology by forcing with observed monthly long-term mean wind stresses, TKE input, and total heat fluxes derived from bulk formulae using monthly long-term mean atmospheric observations combined with model ocean temperature. After the oceanic system has reached an acceptably equilibrated state (gauged by the absence of drift in mean SST and MLD), monthly means of pertinent fields are saved for use in the later experiments.

Using the same strategy as that just discussed, the oceanic salinity field is stabilized to climatological average observations. However, the equilibrium salinity is very sensitive to the evaporation-minus-precipitation $(E - P)$ field, which is not available at present from observations. Hence, we use Newtonian relaxation to the observed annual mean surface salinity field compiled by Levitus (1982) rather than attempting to specify $E - P$.

Spin-up

During a 35-year-long spin-up period, the model was forced by monthly long-term mean fields of atmospheric

wind stress, interpolated from analyses made by the European Centre for Medium-range Weather Forecasting (ECMWF), and total surface heat fluxes (latent, sensible long-wave radiation, and insolation), derived from bulk formulae using model SST and observed atmospheric fields of air temperature (from ECMWF analyses), humidity (COADS), wind speed (ECMWF), and cloudiness (COADS) as inputs. These long-term mean fields, described in Oberhuber (1988), are distinct from the flux and wind-stress anomaly fields, which are formed from individual monthly COADS means as discussed below. Salinity in the surface mixed layer is Newtonially relaxed to Levitus's annual mean observed salinity field so that no evaporation or precipitation fields are needed in the continuity equation.

During the spin-up period, year-to-year changes in SST and mixed-layer depth were monitored to help determine whether the run had developed a reasonable seasonally varying state. Over most of the North Pacific, the SST drift was only a few hundredths of a degree from year 34 to year 35. After the spin-up period was complete, we stored the monthly mean fields of total surface heat flux ($\overline{Q}$) and SST ($\overline{T}_s$) from the final year of spin-up. The field $\overline{Q}$ was used as the mean part of the forcing for all the subsequent runs discussed below. To verify that $\overline{Q}$ was sufficient for mean forcing and to extinguish initial drifts or adjustments in SST, we ran the model for an additional 5 years with $\overline{Q}$ as the surface heat-flux forcing. Since there was little change in mean SST in the North Pacific, the 1970-1988 simulation, outlined below, was commenced from the end of that 5-year period.

Monthly Forcing Fields

Our interdecadal forcing experiments were forced by monthly-mean-plus-anomaly fields of wind stress, total heat flux, and TKE. The wind-stress field is composed of the mean ECMWF analyses, $\overline{\tau}$, plus monthly mean anomalies, τ', derived from the COADS observations. In the extratropics, the COADS wind-stress anomalies are monthly means of the products *wu* and *wv* from individual observations. Drag coefficients were taken from Isemer and Hasse (1987); like the heat-flux exchange coefficients, they are weakly dependent upon wind speed and ΔT. However, since the COADS observations are sparse in the low latitudes, we used anomalies of Florida State University (FSU) wind-stress analyses (Goldenberg and O'Brien, 1981) in the ± 20° latitude zone. In an overlap region, of approximately 10° at 20°N and 20°S, the COADS and FSU flux anomaly fields were smoothly merged.

The TKE variations from month to month were estimated using the observed monthly mean wind speed. We invoked the Weibull parameterization of Pavia and O'Brien (1986) for relating the monthly mean of the wind speed cubed, $\{w^3\}$, to monthly mean wind speed, $\{w\}$, of COADS. Choosing a representative value of this parameterization from the North Pacific regions shown by Pavia and O'Brien yields $\{w^3\} \approx 1.9\{w\}^3$. Comparison of 10 years (1970-1979) of $\{w\}^3$ with $\{w^3\}$ estimated from individual COADS observations exhibits fair agreement: $\{w^3\}/\{w\}^3$ ranged from 1.3 to 2.5 over most 2° squares of the North Pacific. After computing TKE from the monthly mean cubic wind speed and removing the long-term monthly mean, we added the resulting anomalies to the mean ECMWF TKE fields that had been extracted from the model spin-up period.

For the total heat-flux anomalies, we adopted a similar strategy. We used Q' as determined from the COADS observations (after DC1 and the discussion above) poleward of 20° latitude. As described in the Observational Evidence section above, the COADS latent and sensible heat fluxes were formed from monthly averages of products of individual observations. Latent and sensible heat exchange coefficients taken from Isemer and Hasse (1987) are weakly dependent on wind speed and ΔT. In the tropics, ship weather reports are sparse, so we could not easily apply the COADS flux anomalies. However, since there is some evidence that the role of heat fluxes in the tropics is to damp SST anomalies (Liu and Gautier, 1990; Cayan, 1990), we used a Newtonian damping scheme for 20°S to 20°N (in this zone the bulk-formulae flux anomalies are excluded). The Newtonian scheme was formulated as $Q' = \alpha T'$, where T' is the model SST anomaly. The spatially variable parameter α was determined by analyzing the total heat-flux output of the ECHAM T42 model (Roeckner et al., 1992) run that was forced from 1970-1985 with observed SST anomalies. The parameter field α varies geographically over the domain; it was determined by regressing the observed T' with the ECHAM model's Q' output. Typical values of α vary from -10 W m^{-2} °C^{-1} in the eastern tropical Pacific to near -40 W m^{-2} °C^{-1} in the western Pacific.

A point to be made is that the heat-flux parameterizations do depend on the SST, but they do not "build in" the observed SST anomaly variability in the resultant simulation. Actually, the latent and sensible flux formulations depend on the wind speed and the difference $SST - T_a$, which is not well correlated to the SST anomaly. Also, in the governing thermodynamic equation (see equation 4 in the next section), it is the temperature-anomaly tendency, not the anomaly itself, that responds to the flux forcing. Thus, in the simulation the model temperature is free to drift (possibly away from the observed SST state), governed only by the observed heat flux and wind forcings.

Adjustment of the Marine Weather Data

One of the biggest problems with using marine observations is that they contain artificial long-period fluctuations (Cayan, 1990, 1992a; Michaud and Lin, 1992), which cause spurious low-frequency behavior in the fluxes. Specifically,

the marine data contain substantial trends in the most important fundamental variables: wind speed, ΔT, and possibly Δq, even where these data are averaged over the largest spatial scales (DC1). The wind speed trends have been noted by several previous authors (Ramage, 1987; Cardone et al., 1990; Posmentier et al., 1989) and appear to be instrumental artifacts instead of natural variability. Although we were unable to identify a simple instrumental bias responsible for negative trends in ΔT and Δq, we did not trust wholesale decreases in oceanic ΔT and Δq, so we also filtered the ultra-low/large-scale variability from these.

We made two attempts to remove time-varying changes in the fundamental variables involved in the flux calculations. As described in DC1 and above, our first attempt calculated the area-averaged linear trend of w and ΔT, where the area considered was the entire COADS date coverage over the global ocean. Then, the equivalent latent and sensible flux changes were computed for each month of each 5° grid point, by adding the linear change in w and ΔT to their respective long-term monthly means, inserting these into the bulk formulae, and computing the fluxes over 19501988. By subtracting the long-term monthly mean value from each month of the 1950-1988 time history, a "correction" to the latent and sensible fluxes was obtained to reduce the apparent time-varying bias. This version of the fluxes still left apparently spurious low-frequency changes. Further inspection indicated three problems. First, the time-varying bias for ΔT, which generally decreases over time, was *not* linear, but contained low-frequency undulations over the period since 1950. Second, inspection of Δq, which had not been corrected, revealed similar low-frequency fluctuations. (The wind-speed trend, on the other hand, was quite nearly a linear increase of about 1 m s^{-1} over 1950-1988.) Third, changes in the net outgoing terrestrial flux from ΔT trends were not removed in the original correction. (This was because the initial flux-anomaly study focused on variations in the latent and sensible heat components, not the net flux.)

In our second attempt to adjust the flux (Miller et al., 1994a), we more accurately removed the basin-scale low-frequency variation in (generally decreasing) ΔT, by including a similar adjustment for variation (also generally decreasing) in Δq, and retaining the adjustment for w increases. The flux "correction" was calculated in the same manner as before, by perturbing the long-term mean data entering the bulk formulae with the time-varying adjustments. However, in this case, the adjustments to ΔT, Δq, and w were determined from a basin-scale EOF analysis, rather than from a linear trend. The EOF analysis was performed on smoothed versions (13-month running mean filter applied twice) of three COADS data fields encompassing the Pacific basin from 30°S to 60°N and 130°E to 75°W. For each of the three smoothed variables, the spatial pattern of the first EOF exhibited one sign over virtually the entire field. The time coefficients for each of the first EOFs contained the time variation that was portrayed by the linear trend (w increasing, ΔT and Δq decreasing). The first EOFs of the smoothed ΔT, Δq, and w fields accounted for 55 percent, 43 percent, and 73 percent of their variability, respectively. The projection of the first EOF back onto the smoothed data constituted the time-varying adjustments that were then applied in computing the flux corrections.

These adjustments were applied to the respective bulk formulae for the latent, sensible, and net terrestrial (infrared) heat fluxes. Since the first EOF of the smoothed wind speed was very nearly linear and showed relatively little spatial variation, we did not readjust the COADS wind-stress anomalies, which were corrected using the original COADS global-average linear trend of 0.8 m s^{-1} over 1950-1988. These second versions of the corrected fluxes were employed in the "R-run" simulation experiments discussed below.

Mechanisms of SST Variability

To help determine the physical processes forcing SST anomalies, we examine the time variability of the anomalies of the terms in the surface mixed-layer heat budget, along with MLD anomalies and SST anomalies. The surface heat budget is governed by Here the SST (T_s) tendency is balanced by heat-flux input**,** horizontal advection, vertical mixing/entrainment, and diffusion. Q is the net surface heat flux, $\boldsymbol{u}$ is the horizontal velocity, w_e is the entrainment velocity, T_0 is the temperature of the ocean just underlying the mixed layer (whose depth is H), and is the horizontal diffusivity. Monthly means of these quantities are computed during integration, and the climatological monthly means are computed and subtracted from the stored fields to obtain the anomalies.

$$\frac{\partial T_s}{\partial t} = \frac{Q}{\rho c_p H} - \boldsymbol{u}\cdot\nabla T_s - \frac{w_e}{H}(T_s - T_0) + \kappa\nabla^2 T_s \quad (4)$$

The mean and standard deviations of the terms contributing to the heat budget (Equation 4) of the mixed layer are illustrated in Figure 4 for the North Pacific basin, the California Coast, and the central North Pacific. In addition to the heat-flux terms, the mean tendency of SST, the mean and standard deviation of SST, and the mean and standard deviation of MLD are shown for each region. All three regions are heated in spring and summer (April through September) and cool in fall, winter, and early spring (October-March), as indicated by $\frac{\Delta SST}{\Delta t}$. In the climatological mean, the shallowest and deepest MLDs occur in the central North Pacific where the wind forcing undergoes a large annual cycle. This heating and cooling is mirrored by the shoaling and deepening of the mixed layer, which ranges between about 30 m and 150 m. SST and MLD exhibit anomalous year-to-year variability that is a significant fraction of the long-term mean, with typical standard deviations

of 1°C and 20 m, respectively. Of the forcing terms in the heat balance, the heat flux has the largest mean and standard deviation (which is in line with previous studies, e.g., Frankignoul, 1985; Haney, 1985; Luksch and von Storch, 1992), followed by the entrainment. The heat flux is in phase with the climatological mean SST tendency, swinging from positive in spring-summer to negative during fall-winter.

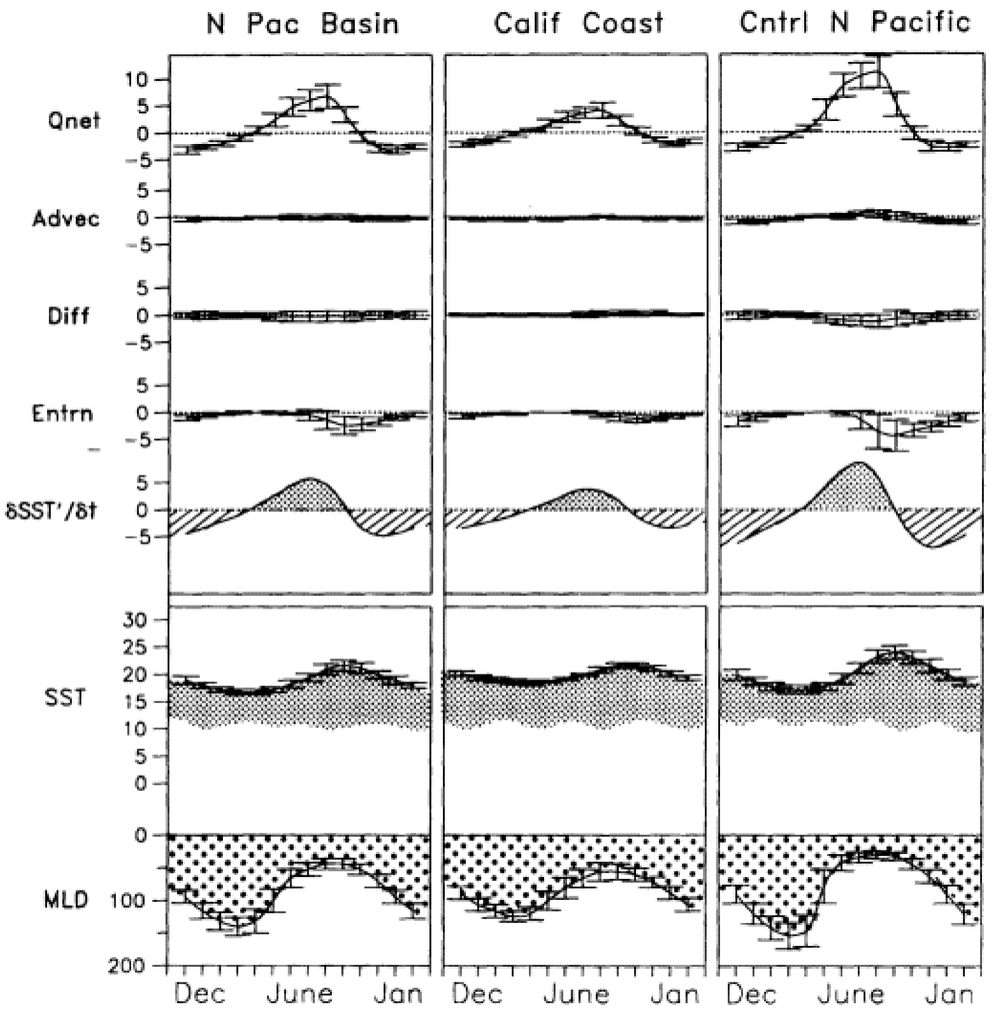

Figure 4
Long-term mean and standard deviation of model heat budget terms $\frac{\Delta SST'}{\Delta t}$, SST (°C), and mixed layer depth (m) for the North Pacific basin, the California Coast, and the central North Pacific regions. Units are 0.1°C mo^{-1} for heat-budget terms and $\frac{\Delta SST'}{\Delta t}$

Entrainment acts only in one direction: to deepen the mixed layer and to cool the temperature. Entrainment exhibits its maximum effect in fall. Presumably this is because the combination of strong winds and a sharp gradient at the bottom of the mixed layer has its greatest potential in fall. Advection, although a small component, acts in phase with the net heat flux in its mean behavior. Diffusion, which acts to dissipate temperature extremes, is out of phase with the SST and about 90° phase-shifted (but usually of opposite sign) from the heating terms.

The spatial pattern of the primary linkages between heat-budget components and $\frac{\Delta SST'}{\Delta t}$ are shown by the maps of the local correlations over the Pacific basin in Figures 5a through 5c, which appear in the color well. Note that $\frac{\Delta SST'}{\Delta t}$ is approximated here by the centered difference between the SST means for the months before and after the month considered. The correlations, calculated separately for heat flux, entrainment, and advection, were obtained for the set of all months of 1970 through 1988. Correlations between heat flux and $\frac{\Delta SST'}{\Delta t}$ (Figure 5a) are relatively high (> 0.6) at nearly all grid points north of 20°N. There is a strong similarity of the model correlations to those derived from observations (Figure 2), with the

strongest correlations (exceeding 0.8) in the lower middle latitudes of the eastern North Pacific and weakest correlations to the northwest, east of Kamchatka. The heat-flux correlations are small in the subtropics, but this is where we prescribed the fluxes to be in phase with the SST via the Newtonian damping scheme. In the tropical Pacific, the correlations are negative and moderately strong, indicating that ocean dynamics processes play a significant role in the model's SST anomaly variability. (Note, however, that the tropical heat flux vs. $\frac{\Delta SST}{\Delta t}$ relationship may be artificial because the fluxes are prescribed using the Newtonian damping scheme.) Interestingly, in data-available regions of the Southern Hemisphere, the correlations again are relatively strong and positive, implying that heat flux is a substantial component of the model's anomalous temperature budget. For entrainment vs. $\frac{\Delta SST}{\Delta t}$ (Figure 5c), fairly high ($\approx$ 0.5) correlations occur at scattered locations poleward of about 10°, and right along the equator. Concerning advection (Figure 5b), greatest correlations (> 0.5) with $\frac{\Delta SST}{\Delta t}$ are found in the subtropics and tropics, with strongest centers developed south of the equator between 5°S and 25°S along South America and between 15°S and 15°N north of Australia in the western tropical Pacific. In the North Pacific extratropics, the correlations are generally not very strong, but there is a mild positive correlation region ($\approx$ 0.4) south of the Aleutian Islands, extending into the Gulf of Alaska.

SST Response: Model vs. Observations

As a first look at the skill of the simulation, we examine the time series of area averages of model and observed SST anomalies (Figure 6). Both model and observed anomalies are defined with respect to their monthly mean climatology for the 1970-1988 time interval. We focus on two key regions plus a North Pacific basin average. One key region is the California Coastal region, bounded by 135° and

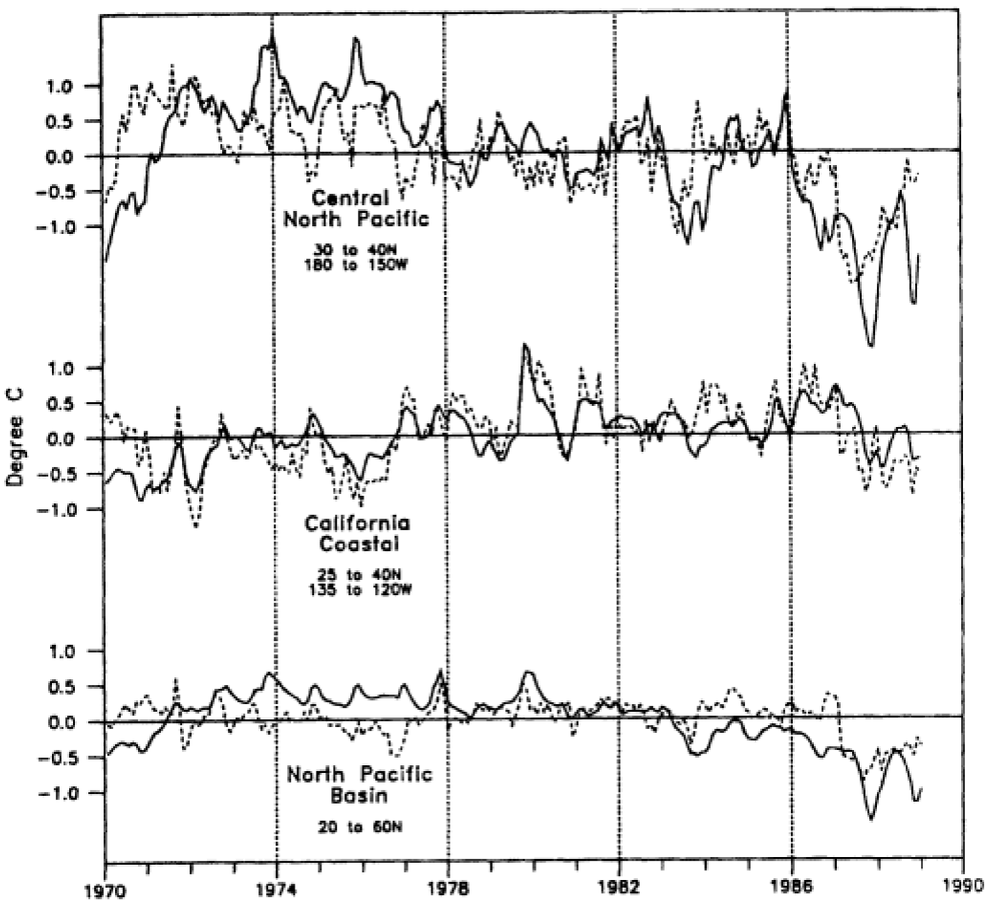

Figure 6
Regional averages of simulated (solid) and observed (dashed) SST anomalies. Correlation coefficients between model and observed are 0.44, 0.71, and 0.67 for the basin-wide, coastal, and central North Pacific regions, respectively.

120°W and by 25° and 45°N, where substantial warming occurred during the 1976-1977 climate shift. The other is in the central North Pacific region, where cooling occurred during the shift, and is bounded by 180° and 150°W and by 30° and 40°N. The basin average was taken in a region corresponding to 130° E to 110°W and 20° to 60°N.

The amplitudes of simulated SST anomalies are slightly lower than the observed anomalies. However, short-term variations in SST, particularly for the coastal region, are remarkably similar considering the uncertainty in the observed heat-flux, TKE, and wind-stress forcing fields. The correlation coefficients between model and observed anomalies are 0.44, 0.71, and 0.67 for the basin-wide, coastal, and mid-Pacific regions, respectively.

Like the observations, the model SST contains variability on monthly to decadal time scales. Reasonable agreement appears in the two key regions, where both major breaks and low-frequency trends are similar. In particular, there is a striking agreement in the longer-time-scale variability, with cooling in the central North Pacific and warming along the Coastal region (Miller et al., 1994a). On the other hand, over the entire North Pacific, the model exhibits a long-term variation in SST, which is not evident in the observations (a residual effect of the long-term variation of heat flux, as described earlier).

The shorter-period model SST variability in Figure 6 has many features in common with the observed SST variability, particularly for the Coastal region. Correlation coefficients between the model and observed SST time series in the central North Pacific and California Coastal regions are 0.67 and 0.71, respectively. In interpreting these, note that the SST contains variability on all time scales, and the correlation is biased toward representing those with the greatest variance. The 1976-1977 warming observed in the Coastal region is clearly evident in the model's response, as is the 1976-1977 cooling of the Mid-Pacific region.

Finally, the spatial pattern of local skill appears in Figure 7 (see color well), which shows the correlation between modeled and observed SST anomalies (all 228 months, 1970-1988). Confirming the validity and impact of the heat flux and wind stress calculated with the bulk formulae, correlations are relatively high (and positive) northward of 20°N, as well as over a broad swath along the tropical Pacific from 165°E to South America. Many grid points exhibit correlations in excess of 0.7. Interestingly, the highest correlations are found in the same area as the largest correlations between the observed latent and sensible fluxes and $\frac{\Delta SST}{\Delta t}$ in Figure 2. Skill is also poor in areas along the western and northern boundaries and just north of the equator near Central America. Although there is a small region of fairly high skill at 40° to 50°S between 120° and 90°W, the model generally performs poorly in the South Pacific extratropics, where data is scarce. Along the immediate tropical strip (5°N to 5°S), the high skill presumably arises primarily from wind-forced ocean dynamics instead of sea-air fluxes. The model skill is low in the region 10° to 20°N of the North Pacific, where the flux was specified using a Newtonian damping instead of from COADS observations. This suggests that the idealized Newtonian flux scheme is not realistic, and supports the validity of the bulk-formulae fluxes.

For better understanding of the forcing of the anomalous heat budget, $\frac{\Delta SST}{\Delta t}$ was correlated with monthly anomalies of each of the terms on the right-hand side of Equation 4, with the sum of these four terms, and with the MLD anomaly. Results are shown in Figure 8 for the averages over the North Pacific basin, the California Coastal region, and the central North Pacific region. The relationships in the three regions are quite similar. Consistent with the maps shown in Figure 5, the strongest influence on the mixed-layer temperature anomaly is the net heat-flux anomaly, with correlations usually exceeding 0.7. The next most important term is entrainment, which is important when the mixed layer begins to deepen, and the heat accumulated in summer is vented to the atmosphere. Correlations of $\frac{\Delta SST}{\Delta t}$ and entrainment are greatest in fall and early winter, some exceeding 0.8. The correlations with entrainment are lowest in spring when mixed-layer depth is decreasing, and remain low until fall when it begins to deepen again. Advection is not as strongly correlated with $\frac{\Delta SST}{\Delta t}$ as the heat flux and the entrainment are, but advection does exhibit correlations exceeding 0.5 in winter for the central North Pacific and

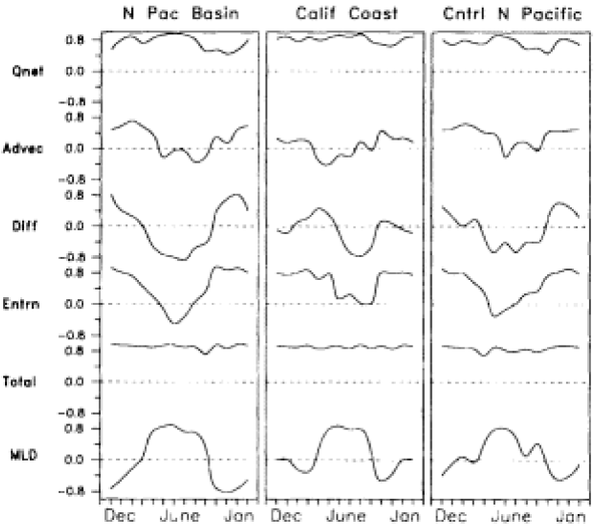

Figure 8
Correlation between $\frac{\Delta SST}{\Delta t}$ and: each of the anomalous model heat-budget forcing terms (right-hand side of Equation 4); their total; and anomalous MLD for the North Pacific basin, California Coastal, and central North Pacific regions. Stratified by month, from 1970-1988.

North Pacific basin regions during winter. Model advection is generally not an important influence on SST anomalies in the Coastal region. There is an interesting seasonal cycle in the link between MLD and $\frac{\Delta SST}{\Delta t}$, which has its strongest expression for the North Pacific basin average. In fall-early winter (October-January), the two are out of phase: The SST anomaly tends to decrease ($\frac{\Delta SST}{\Delta t}$ is negative) when the mixed layer is anomalously deep, and vice versa. This implies that when large heat losses and strong wind mixing produce decreasing winter SST anomalies, they also produce a deeper MLD. In summer, the sign of the relationship reverses: The SST anomaly tends to increase when the mixed layer is anomalously deep. This suggests that in summer, when MLD is shallow, the mechanisms that extract heat from the mixed layers produce decreasing SST anomalies when the layer is thinner and the gradient below the mixed layer is stronger (and vice versa).

Analogous correlations (not shown) were also computed for the Niño 4, Niño 3, and Niño 2 regions along the equator from the international date line to South America. The largest contributions to model SST-anomaly variability in these equatorial regions are entrainment, advection, and diffusion. Strong correlations linking equatorial Pacific SST anomalies to advection and entrainment are indicated by the maps in Figures 5b and 5c. In the tropics, SST anomaly tendencies are generally in phase with MLD anomalies (warming coincides with deeper mixed layers), but not strongly so.

The 1976-1977 SST Shift

To evaluate the model's performance in simulating the spatial pattern of the 1976-1977 shift, the wintertime SST difference field for the six years after the shift (December 1976-February 1977 through December 1981-February 1982) minus the six years before the shift (December 1970-February 1971 through December 1975-February 1976) was calculated, following Graham (1991). Figure 9 (see color well) shows these fields, with the observed SST differences for comparison. The model captures the principal extratropical observations, namely, a warming in the Coastal region and a cooling in the Mid-Pacific region. In the tropics and subtropics, observations contain a swath of warm water throughout the equatorial region and across the southeastern North Pacific. The model captures only a vestige of this warming, which appears mostly in the western half of the tropics. This discrepancy may relate to the use of Newtonian damping rather than observed fluxes in the ± 20° zone. The warming in the equatorial Pacific points to possible dynamic effects due to wind-stress anomalies alone. Mechanisms for the SST shift are suggested by the comparable-difference maps of the winter fields of SLP, net heat flux, and pseudo-rate of kinetic energy transfer by the wind shown in Figures 10a, 10b, and 10c. These maps clearly show a deepened winter Aleutian Low during the post-1976 period (see also Venrick et al., 1987; Trenberth, 1990; Trenberth and Hurrell, 1995, in this volume). The deepened low sustained stronger winds and greater storm activity across the central North Pacific, and generally warmer, moister air masses along the West Coast. This pattern represents a tendency for strong positive PNA patterns in the post-1976 period. These conditions resulted in a large region of increased heat loss in the western and central North Pacific and decreased heat loss in the eastern North Pacific. Increased wind mixing apparently occurred in the central North Pacific, particularly between 30° and 40°N along the southern fringe of the anomalous low-pressure center. Both the heat-flux and wind-mixing patterns are consistent with the SST difference field, shown in Figure 9. Also, the heat-flux difference map is quite similar to the latent-and-sensible heat-flux anomaly maps associated with months having large PNA EOF amplitudes, which appear in Figures 1 and 3.

Inspection of the seasonal time series of the heat-budget components at the individual regions helps to understand

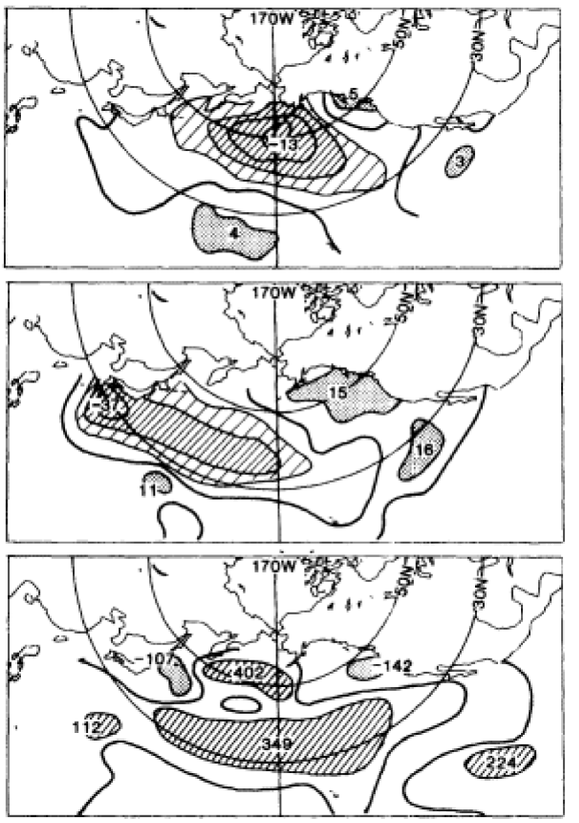

Figure 10
Difference fields of observed winter SLP (mb; top), heat flux (W m^{-2}; middle), and $\{w^3\}$, the pseudo-total kinetic energy (m^3 s^{-3}; bottom), for the winters of 1976-77 through 1981-82 minus those of 1970-71 through 1975-76.

the evolution of variability features such as the 1976-1977 shift (Miller et al., 1994a,b). In the Coastal region, heat-flux input tends to be about four times larger than either horizontal advection or entrainment effects. In the mid-Pacific region, in contrast, which is nearer the more variable winds of the storm track, heat-flux input is only twice as large as horizontal advection, and typically the same as entrainment effects. Diffusion tends to be slightly weaker than horizontal advection, but inspection of the time series shows that diffusion simply acts in opposition to the cumulative effects of the other heating term.

During the six-month period preceding the 1976-1977 climate shift, a long period of warming via heat-flux input occurred in the Coastal region (not shown). Although this period was not particularly strong, it was persistent compared to most of the rest of the time intervals (Miller et al., 1994a). What makes this period particularly striking, however, is that the strongest occurrence (in the 1970-1988 time interval) of warming by horizontal advection took place during fall 1976 and the subsequent winter. Together, these two effects resulted in a mixed layer 10 to 15 m shallower and more than half a degree of warming in the surface temperature. In spite of a strong loss of heat during the late winter of 1977, the system managed to remain in a shallow mixed-layer, warm-SST state through the winter of 1988. Throughout 1977, several months of strong heat-flux cooling began to cool the upper ocean toward the mean, but strong heating in summer 1979 thinned the mixed layer and warmed the SST to such a degree that the mixed-layer warmth persisted into winter 1980.

In the Mid-Pacific region, the 1976-1977 climate shift is likewise instigated by the effects of an anomalously long and strong period of cooling by horizontal advection combined with sizable cooling by heat flux (Figure 11). During the six-year period preceding the shift, anomalously weak entrainment effects (partially due to lower TKE input) serve to maintain the system in a shallow mixed-layer, warm-SST state. In the years following the shift, the effects of stronger entrainment are confined to the summer months.

It therefore appears that the 1976-1977 shift in both the Coastal and Mid-Pacific regions was caused by an unusual atmospheric state that took hold several months before the 1976-1977 winter, and by conditions in the winter atmospheric circulation that persisted for several winters thereafter. This atmospheric circulation produced large-scale shifts in ocean-current advection that acted in concert with large-scale heat-transfer processes to significantly alter the upper-ocean thermal structure, and thus its stratification. The Mid-Pacific region subsequently remained in that perturbed state through the maintenance effects of reduced TKE input.

SUMMARY AND DISCUSSION

Two experimental approaches indicate that bulk parameterizations yield fairly realistic estimates of anomalous sea-air fluxes on seasonal-to-interannual scales over the tropical and northern extratropical oceans. Monthly parameterizations of wind stress and heat flux derived from COADS historical summaries provide reasonable coverage over much of the Pacific basin back to the 1960s. The validity of these derived variables was demonstrated in two ways: (1) by the consistency of the spatial and temporal variability of heat-flux anomalies with independently observed data on the atmospheric circulation and SST tendency; and (2) by the success in simulating two decades of Pacific Ocean SST anomalies with a model driven by the parameterized wind and heat-flux forcings. The bulk parameterizations appear to be adequate for useful diagnoses of several unobserved thermal and dynamic processes (advection, vertical mixing, etc.) that operate in the upper ocean on seasonal-to-decadal time scales.

The model's air-sea heat fluxes were shown to be consistent with two sets of independently observed data. First, the latent and sensible flux anomalies are spatially organized by the atmospheric circulation into systematic patterns about the major cyclonic and anticyclonic features. This organization occurs because the fluxes are determined by wind speed and by air-mass temperature and humidity, which have characteristic structures relating to the general circulation. The flux anomaly/circulation patterns that appear in the North Pacific are confirmed by very similar patterns found

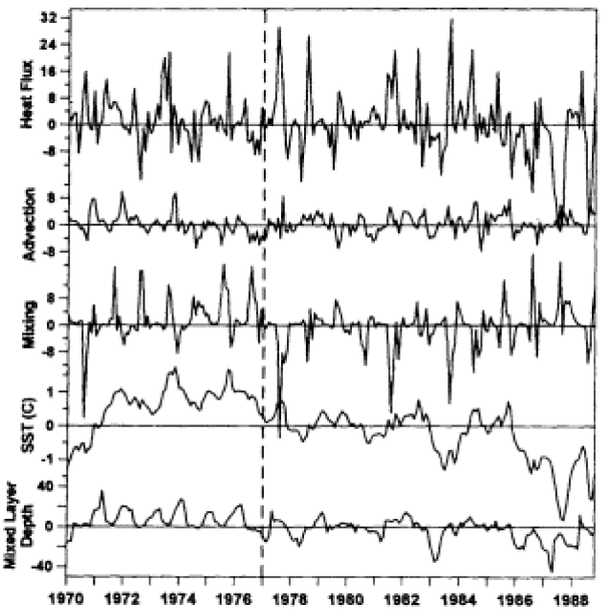

Figure 11
Monthly anomaly time series (1970-1988) of simulated surface heat-budget components (net heat-flux term, horizontal advection term, and entrainment term), along with simulated mixed-layer depth (m) and SST (°C), for the central North Pacific. Dashed vertical line marks January 1977, the approximate time at which the large North Pacific SST shift occurred.

in the North Atlantic (not shown, but see DC1 and DC2). Second, the modeled latent and sensible heat-flux anomaly patterns correspond well to those of SST anomaly tendencies, with regions of increased sea-to-air heat exchange overlying regions of decreasing SST, and vice versa. Monthly SST anomaly tendencies have typical magnitudes of 0.3°C mo^{-1}, and correspond to monthly mean flux anomalies having typical magnitudes of 50 W m^{-2}. Together, the magnitudes of the heat flux and SST tendency are consistent with observed mixed-layer depths.

We also tested the ability of monthly heat fluxes and winds to force a Pacific Ocean general-circulation model over an extended period (1970-1988). The forcings were monthly means of the bulk-formula parameterizations; in this experiment, we superimposed the monthly *anomalies* of the fluxes and wind parameterizations upon the climatological forcing that was used to spin up the model to its "stable" annual cycle. In general, the simulation agreed well with observed SST where weather reports (wind, temperature, and humidity) were densely sampled in the extratropical region north of 20°N, but compared quite poorly where they were sparsely sampled. Model SST-anomaly performance was best in the eastern North Pacific between 20°N and 40°N, and along the equatorial strip. It performed poorly between 5°N and 20°N, in the western tropical Pacific, and in most of the southern Pacific. Miller et al. (1994a) showed that the model was remarkably successful in simulating the first three empirical modes of the winter North Pacific SST anomaly.

In the model, anomalous heat fluxes and wind-driven entrainment provide the primary extratropical forcing of the upper-ocean thermal field. The model clearly shows that in the extratropics, the mixed layer deepens with winter anomalous cooling, and shoals with anomalous warming. SST in the region from 5°N to 20°N was poorly simulated, probably because of poor representation of the heat-flux anomalies by a Newtonian scheme in the ± 20° strip. Near the equator, however, where SST anomalies reflect ocean dynamic response to wind forcing, the model anomalies closely resembled those observed.

At lower temporal frequencies, the model captures some important elements of the interannual-to-decadal variability, including aspects of the marked Pacific-basin "shift" that occurred in the winter of 1976-77. Multiple causes appear to be at work in creating the shift, including horizontal advection, anomalous heat fluxes, and wind stirring. This result suggests that a major portion of the shift was forced locally (albeit organized over a large scale) by the atmosphere, rather than by an internal adjustment of the ocean's thermal field. The latter mechanism deserves closer attention, since it is a prime candidate for driving the North Pacific decadal variability exhibited in recent coupled ocean/ atmosphere model results of Latif and Barnett (1994).

These results suggest that ocean models forced by parameterized monthly surface observations are capable of generating important aspects of the anomalous SST variability, on monthly to multi-year time scales. Evidently the lack of synoptic weather variability that characterizes real winds and fluxes is not fatal to the model results. Note, however, that synoptic effects are aggregated into the monthly averages of the fluxes and wind stress, as the nonlinear products within the bulk formulae are taken on an observation-by-observation basis. A more sensitive issue in the simulation of decadal and longer ocean histories is the treatment of the lowest frequencies of the marine data. In the model run conducted here, we removed the largest-spatial-scale, low-frequency (trend-like) behaviors in the wind speed, ΔT, and Δq, since these seemed likely to have arisen from instrumental artifacts. This issue is problematic, though, and longer model runs will be needed to further test these assumptions.

Commentary on the Paper of Cayan et al.

STEPHEN E. ZEBIAK
Lamont-Doherty Earth Observatory

I think Dr. Cayan has given us the opportunity to consider a lot of fairly serious questions, particularly in relation to decadal time scales and ocean modeling. I have noted a few questions that came to my mind. Some of them are really quite general questions, but perhaps they can focus our discussion.

My first two points really deal with the whole issue of using surface heat fluxes for ocean modeling purposes. Dr. Cayan talked about the issue of biases, and I think that when we come to consider decadal time scales, this is an overwhelmingly big problem. The technique that he used was to take components of the flux fields, subject them to EOF analyses, and to look at the first mode and essentially take it out.

I wonder whether we can come to some agreement as to whether that is the best way to proceed. For instance, some of the other talks, such as that of Dr. Wallace yesterday, viewed some of the first empirical orthogonal factors